Energy & Buildings 264 (2022) 112065

Contents lists available at ScienceDirect

Energy & Buildings

journal homepage: www.elsevier.com/locate/enb

Modeling and optimization of hybrid ground source heat pump with district heating and cooling

Anjan Rao Puttige *, Staffan Andersson, Ronny Östin, Thomas Olofsson

Umeå University, Umeå, Sweden

ARTICLE INFO

Article history:
Received 21 July 2021
Revised 21 February 2022
Accepted 26 March 2022
Available online 30 March 2022

Keywords:
Ground source heat pump
District heating and cooling
Optimization
Borehole heat exchanger
Artificial neural network
Hybrid model

ABSTRACT

Hybrid heating systems with ground source heat pumps (GSHP) and district heating and cooling offer flexibility in operation to both building owners and energy providers. The flexibility can be used to make the heating system more economical and environmentally friendly. However, due to the lack of suitable models that can accurately predict the long-term performance of the GSHP, there is uncertainty in their performance and concerns about the long-term stability of the ground temperature, which has limited the utilization of such hybrid heating systems. This work presents a hybrid model of a GSHP system that uses analytical and artificial neural network models to accurately represent a GSHP system's long-term behavior. A method to improve the operation of a hybrid GSHP is also presented. The method was applied to hospital buildings in northern Sweden. It was shown that in the improved case, the cost of providing heating to the building can be reduced by 64 t€, and the CO_2 emissions can be reduced by 92 tons while maintaining a stable ground temperature.

1. Introduction

Heating and cooling account for half of the energy use in Europe [1]. Two-thirds of the heating is still provided by fossil fuel based boilers [2]. Therefore, the decarbonization of the heating and cooling sector is an essential part of the strategy to reach the European Union's goal of reducing annual greenhouse gas emissions by 80% compared to 1990. Electrification of heating and cooling through heat pumps and district heating and cooling (DHC) are strategies to achieve this goal [2,3]. In Sweden, both DHC and heat pumps have a significant market share [4,5]. District heating is the dominant heating option in urban areas, especially multi-family buildings, where about 90% of the heat comes from district heating [4]. A variety of heat pumps is primarily used in suburban and rural single-family buildings. According to [6], 20–25% of single-family houses use a ground source heat pump (GSHP) system. Improvements in heat pump technology and increasing efficiency of buildings have increased the competitiveness of GSHP systems in markets typically dominated by district heating [6]. In recent years, the number of GSHPs in larger residential and commercial buildings have increased and GSHP is considered as a serious competitor to district heating and cooling [4,7].

However, if GSHP systems are considered as an asset in the district heating and cooling networks, the GSHPs can be operated in such a way that both the building owners and the energy utility companies benefit from cooperation. There is a natural synergy between heat pumps and district heating from combined heat and power plants that makes the inclusion of heat pumps in district heating and cooling networks advantageous [5]. GSHP systems, in particular, can be used to handle increased variation in future energy systems by storing excess energy [8]. Several examples demonstrate that GSHP systems can increase the utilization of waste heat [9], solar thermal energy [10,11], and wind energy [12]. Under the right conditions, hybrid GSHP and district heating and cooling systems can be profitable for both building owners and energy utility companies; therefore, energy companies should specifically address such systems [13].

Buildings with multiple heating options have the flexibility to choose the combination of the most beneficial heating options. Determining the optimal distribution of load among the heating options is not a trivial problem. There are several studies on the design and operation of such systems [14–18]. Distribution of load is particularly hard when GSHP is part of the heating system since the heat extracted or injected into the ground can affect the performance of the GSHP for many years. Therefore, the optimal operation of a GSHP system must consider the long-term stability of the ground in addition to the short-term coefficient of performance (COP).

* Corresponding author.
E-mail address: anjan.puttige@umu.se (A.R. Puttige).

https://doi.org/10.1016/j.enbuild.2022.112065
0378-7788/

Nomenclature

r_b	Borehole radius (m)
H	Active length of borehole (m)
D	Ground water level (m)
K	Thermal conductivity of the ground $W(mK)^{-1}$
ρCp	Volumetric heat capacity $(JK^{-1}m^{-3)}$
R_b	Borehole resistance (mKW^{-1})
T_{ug}	Undisturbed ground temperature (°C)
CompPower	Electric power of the compressors (W)
HPCoolPower	Cooling effect of the heat pump (W)
HPCoolmf	Flow rate in the cooling side of heat pump (m^3/h)
HPHeatTout	Outlet temperature of water from the heating side of heat pump (°C)
HPCoolTin	Inlet temperature of water for the cooling side of heat pump (°C)
BY10Power	Space heating load of building number 10 (W)
BY23Power	Space heating load of building number 23 (W)
BYCoolTin	Inlet temperature of HXC on the building side (°C)
BYCoolTout	Outlet temperature of HXC on the building side (°C)
CoolTin	Inlet temperature of HXC on the heat pump side (°C)
CoolTout	Outlet temperature of HXC on the heat pump side (°C)
DHWPower	Domestic hot water load (W)
DHWTout	Outlet temperature of domestic hot water from the heat pump (°C)
BHATin	Inlet temperature of Borehole group A (°C)
BHATout	Outlet temperature of Borehole group A (°C)
BHBTin	Inlet temperature of Borehole group B (°C)
BHBTout	Outlet temperature of Borehole group B (°C)
BHAmf	Flow rate of borehole group A (m^3/h)
BHBmf	Flow rate of borehole group B (m^3/h)
ExcessTout	Outlet temperature of HXH on the BHE side (°C)
BHAP	Heat extraction rate of borehole group A (W)
BHBP	Heat extraction rate of borehole group B (W)
CoolPower	Cooling demand of the building (W)
U	Overall heat transfer coefficient $(Wm^{-2}\ K^{-1})$
A	Effective area of the heat exchanger (m^2)
LMTD	Log mean temperature difference (°C)
PowerBalanceCC	Power balance of the cold circuit (W)
CoolTinReq	Required value of CoolTin (°C)
DCoolTin	Difference between required and predicted CoolTin (°C)
COPCool	Coefficient of performance of heat pump for cooling
COPHeat	Coefficient of performance of heat pump for heating
ϵ	Penalty cost for long term stability of the ground (€/MWh)
BHP	Heat extraction rate of borehole heat exchanger (W)

Abbreviations

GSHP	Ground source heat pump
DHC	District heating and cooling
COP	Coefficient of performance
BHE	Borehole heat exchanger
DST	Duct storage
FLS	Finite line source
ILS	Infinite line source
ANN	Artificial neural network
HXC	Cooling heat exchanger
HXH	Excess heat exchanger
SP1	Set Point 1
SP2	Set point 2
SP3	Set Point 3
MAE	Mean absolute error

Developing a borehole heat exchanger (BHE) model that is accurate in both the long-term and short-term is challenging. The problem is generally solved by using a separate model for the ground around the borehole, which represents the long-term behavior of the ground, and for inside of the borehole, which represents the short-term behavior. Many long-term models are based on a pre-calculated non-dimensional response function for the BHE, called g-function [19]. The g-functions can be calculated using several analytical [20–25] or numerical models [26,27] with varying degrees of accuracy and complexity. The g-function approach assumes that all the boreholes are connected in parallel with a single inlet temperature. Hence models that considered multiple inlets were developed [28–31]. Short-term models are either based on representing the inside as a network of thermal resistors and capacitors [32–35] or by simplifying the heat transfer problem to find the exact solution [36–41]. Numerical approaches have also been used for short-term models [42,43], since these models do not consider the interaction between the boreholes they are not accurate in the long term. For a model to be accurate in both the short and long term, long-term and short-term approaches can be combined to represent the BHE.

During the optimization of heating systems with GSHP, many studies ignore the variation in ground temperature by considering the COP of the GSHP as a constant [14,16] or the ground temperature as constant [15]. Other studies ignore the long-term temperature variation in the ground using only short-term models [44] or using empirical parameters from short experiments [45]. The performance of the GSHP system will deteriorate over time if the load of the BHE is not balanced, i.e., if the annual heat injected into the BHE is not zero, which can make the load distribution sub-optimal in the long term. Many studies represent the ground using duct storage (DST) [43] model used in the commercial software TRNSYS [11,46,47]. The DST model is limited as it does not include interaction between the boreholes and hence cannot represent the long-term behavior of the BHE, and it assumes a uniform distribution of boreholes in a BHE. Rohde et al. [42] implemented a similar model in Modelica and used it to optimize the supply temperature of a heating system with BHE [48]. Other simple models for BHE that do not consider the short-term behavior, like the finite line source (FLS) model [17] and infinite line source (ILS) model [18], have also been used. Few studies use an accurate representation of both the ground and inside of the borehole. Ruiz-Calvo et al. [49] presented a short-term model that was combined with a long-term g-function model and implemented in TRNSYS. The model was applied to compare operation strategies of a dual-source heat pump, but a long-term simulation of the model was not performed. Li et al. [50] used a combination of analytical g-function and a resistance–capacitance model to represent a BHE. They studied the feasibility of using water tanks and BHE to store energy from a data center. They studied different scenarios but no optimization was performed. Figueroa et al. [51] presented an approach based on model predictive control with a long prediction horizon to optimize a hybrid GSHP system. The approach divides the total prediction time into short-term and long-term (shadow cost) periods with larger time steps in the long-term period. The application of such a model to larger installations may not be practical due to high computational time.

Artificial neural network (ANN) are data-driven models that consists of multiple layers of a simple processing unit called nodes with weighted interconnections. ANNs use training data to learn the relationship between the inputs and outputs in complex systems. The use of ANNs to model heating and cooling in buildings has gradually increased in recent decades [52,53]. ANN has been used to model GSHP systems [54–56] and BHE [57–59]. The authors presented a hybrid analytical-ANN model for BHE that can accurately represent both the short-term and long-term behavior of the BHE [60]. We also showed that ANN models are more accurate than typical empirical models of heat pumps when data from actual operation is available [61].

The objective of the present study is to demonstrate the use of models to improve the operation of GSHP systems operating in parallel to DHC networks. We aim to improve the operation by ensuring a balanced operation of the BHE. Therefore, we ensure that the potential of the geothermal source does not decrease over time. BHE are a major investment in a GSHP system, therefore protecting this investment and preventing deterioration of the GSHP system performance is important. Additionally, we aim to reduce the annual operating cost of heating and cooling the building from the perspective of the energy provider. The perspective of the energy provider was chosen since they supply the energy to the building owner, hence a reduction in cost for the energy provider can be transferred to the building owners too. By quantifying the economic benefit and assuring good long-term operation of the GSHP this study promotes better cooperation between the energy company and the building owners. A case study of a hospital area in northern Sweden is used. The heating and cooling demands of the area are satisfied using a local GSHP and DHC network. A description of the case study is presented in section 2. Sections 3.1–3.3 presents a description of the component models. Section 3.4 presents a model for the entire GSHP system using an ANN model for the heat pump and a hybrid analytical-ANN model for the BHE. A method to distribute the load between the GSHP and DHC network to reduce the operating cost of the energy company while maintaining a stable temperature in the ground is presented in section 3.5. The results of the study are presented in section 4 followed by a discussion of the results in section 5. The main conclusions of the study are presented in section 6.

2. Description of the installation

In this work, we have developed models and used them to optimize the operation of a GSHP system at the university hospital in Umeå, Sweden. The GSHP is used for both heating and cooling along with the district heating and cooling network. The GSHP system was designed to cover 95% of the cooling demand in the buildings (5 GWh) and 20% of the heating demand (7 GWh). The designed heating and cooling load is 1124 kW and 964 kW, respectively. Fig. 1(a) shows a schematic of the heating and cooling system of the hospital area. GSHP is connected to the cooling network of all the buildings in the hospital, while it is connected to only two of the buildings in the hospital area for heating. Cooling is a yearly demand in some areas of the hospital buildings, and thus heating and cooling demands may occur simultaneously.

The GSHP system consists of 3 heat pumps and 125 boreholes. Fig. 1(b) shows a schematic of the GSHP system. Two of the three heat pumps are used for heating and cooling. Each of the two heat pumps has four compressors operating in parallel. The third heat pump is used for domestic hot water and for heating during the coldest periods. A detailed explanation of the heat pumps can be found in [61]. The boreholes are divided into two groups, A and B, with independent fluid loops. The boreholes have a depth of 200/250 m, and the distance between the boreholes is 7 m. The properties of the boreholes are summarized in Table 1, and further details can be found in [63].

2.1. Modes of operation

Fig. 2 shows schematics of the GHSP-system in (a) heating mode and (b) cooling mode. Note that the 3-way valve 3WVC is completely open in heating mode and, therefore, not shown in Fig. 2b. In the heating mode, the GSHP is controlled by the heating demand, and cooling is a by-product. There are two heating modes; BHE in parallel to the cooling heat exchanger (HXC), and BHE in series to HXC. The BHE in parallel to HXC mode is used in winter operation when the cooling emission from the heat pump is higher than the cooling demand, and thus cold can be stored in the BHE. The three-way valve (3WVC) adjusts the flow rate to HXC such that the required temperature is maintained at BYCoolTin, which is typically 8 °C. The remaining flow is directed into the BHE, which stores the excess cold. The BHE in series to HXC mode is used in spring and autumn operations when the cooling demand is comparable to the cooling emission from the heat pump. When BHE operates in series with HXC, the flow through HXC is controlled by 3WVC, but the entire mass flow is directed into the BHE. This operation will either inject or extract heat from the ground depending on the inlet temperature and the ground temperature.

In the summer (cooling mode), the GSHP is controlled by the cooling demand, the heat released is used for heating, and the excess heat is stored in the ground by the heat exchanger, HXH. The 3-way valve 3WVH controls the mass flow rate through HXH to obtain the required outlet temperature from the heat pump at HPHeatTout, which is typically 40 °C. The cooling operation also has two modes; free cooling with active cooling mode and active cooling mode. In the former case, the borehole group A is connected to the heat exchanger HXH to absorb the excess heat, while borehole group B is operating in series with the heat exchanger HXC to provide free cooling. In the active cooling mode, both the borehole groups are connected to the heat exchanger HXH and the cooling demand is supplied by the heat pump alone.

Variable pumps control the flow rate in the heating and cooling circuit. The speed of the pumps is decided based on the number of compressors switched on in the heat pumps. Therefore, the flow rate in the heating and the cooling circuit is decided based on the compressor power levels. Separate circulation pumps control the flow rate in the BHE. When the boreholes are connected to the cooling side, the circulation pumps are controlled to minimize the flow through the bypass BP. When the boreholes are connected to the heating side through the heat exchanger HXC, the circulation pumps are controlled to absorb the excess heat from the heat pump and maintain the temperature at ExcessTout.

Thus, the GSHP-system has four modes, heating with BHE in parallel to HXC, heating with BHE in series to HXC, free cooling with active cooling, and just active cooling. The mode changes from heating with BHE parallel to active cooling as the dominant demand changes from heating to cooling. Fig. 3 summarizes the switches between the modes of operation as the demand changes.

After the first few years of operation, the operator of the GSHP observed that the temperature of borehole group A was increasing over the years. Therefore, the operator decided to manually change the mode from free cooling with active cooling to active cooling for a few days in the summer to limit the increase in temperature. Hence, from the summer of 2019, the active cooling mode was used for a few days even if the criteria for shifting the mode were not satisfied.

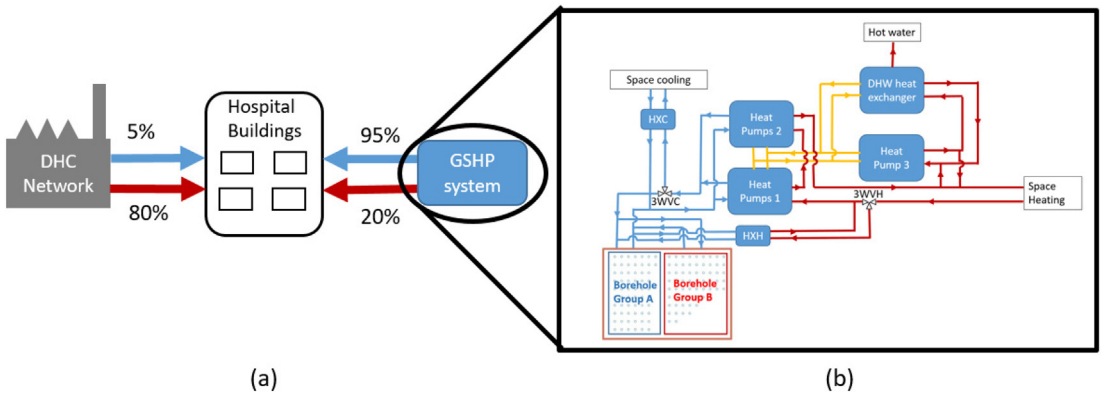

Fig. 1. (a) Heating and cooling system in the hospital area (b) Schematic of the GSHP system (adapted from [62]).

Table 1
Properties of BHE.

Property	Value
Borehole radius (r_b)	0.070 m
Borehole depth (H + D)	200 m/250 m
Ground water level (D)	10 m
Thermal conductivity of the ground (k)	3.4 W(mK)$^{-1}$
Volumetric heat capacity of the ground (ρCp)	2.3 MJK^{-1} m^{-3}
Borehole resistance (R_b)	0.08 mKW^{-1} (0.11 mKW^{-1} for extraction)
Undisturbed ground temperature (T_{ug})	5.9 °C

2.2. Measurements

The GSHP has been in operation since February 2016, and the monitoring system was installed in January 2017. However, the flow and energy meters for the borehole groups were installed in March 2017. In this study, we used four years of monitored data from the GSHP. Table 2 shows the list of measurements used in this study, and Fig. 4 shows the positions of the sensors. Data from other sensors were not used as they were either redundant or irrelevant.

The hourly average measured values from 2017-05-01 to 2021-04-30 are used in this study. The period contains 35,064 h, but one or more measures are faulty for a total of 4208 h. Therefore, 30,856 h of measured data is used. Some faults were detected by manually examining the data; for example, the difference between CoolTin and CoolTout was very low from 2020-12-12 to 2021-01-21. Other irregularities in the data points were eliminated based on some simple rules; for example, BYCoolTout must be greater than CoolTin. The power from the power meter must be comparable to the power calculated from the temperatures and the mass flow rates. Note that HPCoolPower is considered as positive when the heat pump extracts heat from the cooling circuit, and BY10Power and BY23Power are considered positive when heat is transferred from the heating circuit to the building.

3. Model description and optimization

We developed models for BHE, heat pump, and heat exchanger (HXC) using the measured data. Each of the models was developed independently. A model of the GSHP system was then developed by combining the individual models. The system model was used to optimize the operation of the GSHP system. The hybrid model presented in [60] for the BHE was adapted and trained using the measured data described in section 3.1. An ANN model for the heat

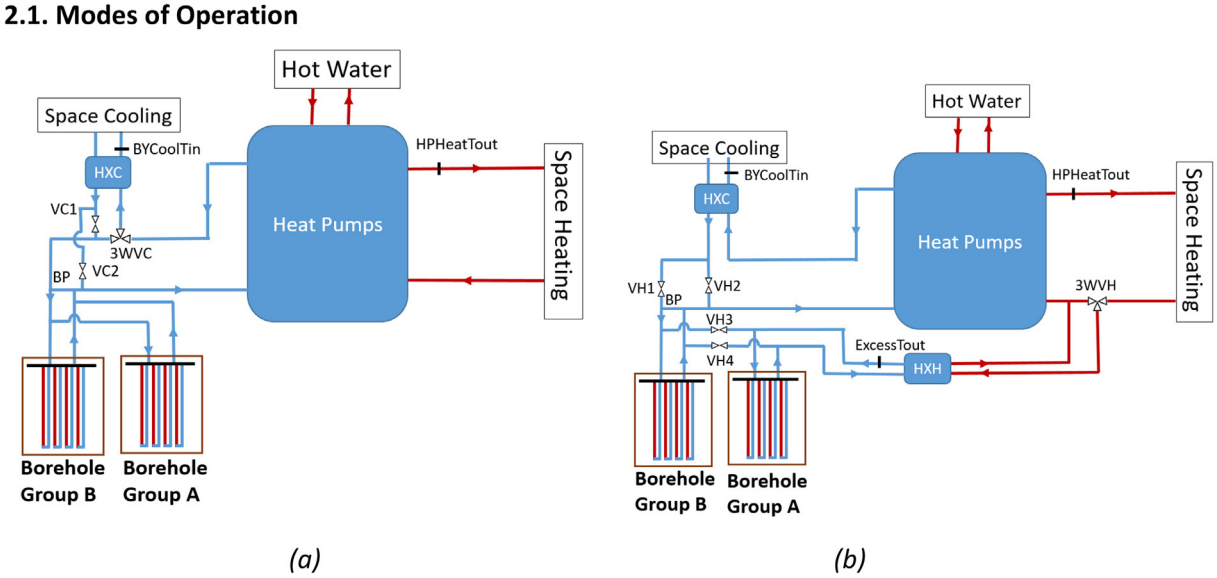

Fig. 2. Schematics of the GHSP-system in (a) heating mode and (b) cooling mode.

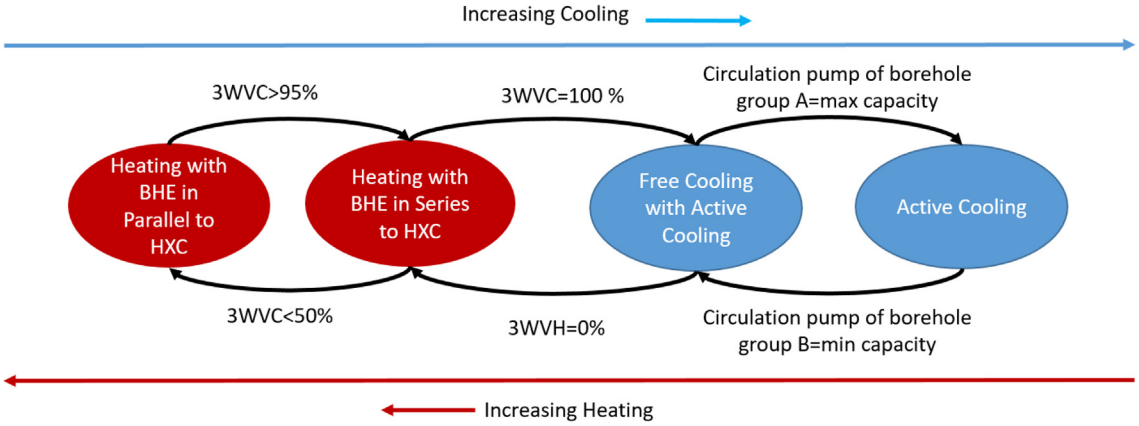

Fig. 3. Criteria for change in modes of operation.

Table 2
List of measurements used in this study.

Component	Measurement	Description	Units	Position in Figure
Heat pump	CompPower	Electric power of the compressors	kW	1
	HPCoolPower	Cooling effect of the heat pump	kW	2
	HPCoolmf	Flow rate in the cooling side of heat pump	m^3/h	3
	HPHeatTout	Outlet temperature of water from the heating side of heat pump	°C	4
	HPCoolTin	Inlet temperature of water for the cooling side of heat pump	°C	3
Heating	BY10Power	Heating load of building number 10	kW	5
	BY23Power	Heating load of building number 23	kW	5
Cooling	BYCoolTin	Inlet temperature of HXC on the building side	°C	6
	BYCoolTout	Outlet temperature of HXC on the building side	°C	7
	CoolTin	Inlet temperature of HXC on the heat pump side	°C	8
	CoolTout	Outlet temperature of HXC on the heat pump side	°C	9
Domestic hot water production	DHWPower	Domestic hot water load	kW	10
	DHWTout	Outlet temperature of domestic hot water from the heat pump	°C	11
Borehole heat exchanger	BHATin	Inlet temperature of Borehole group A	°C	12
	BHATout	Outlet temperature of Borehole group A	°C	13
	BHBTin	Inlet temperature of Borehole group B	°C	14
	BHBTout	Outlet temperature of Borehole group B	°C	15
	BHAmf	Flow rate of borehole group A	m^3/h	12
	BHBmf	Flow rate of borehole group B	m^3/h	14
Excess heat exchanger	ExcessTout	Outlet temperature of HXH on the BHE side	°C	16

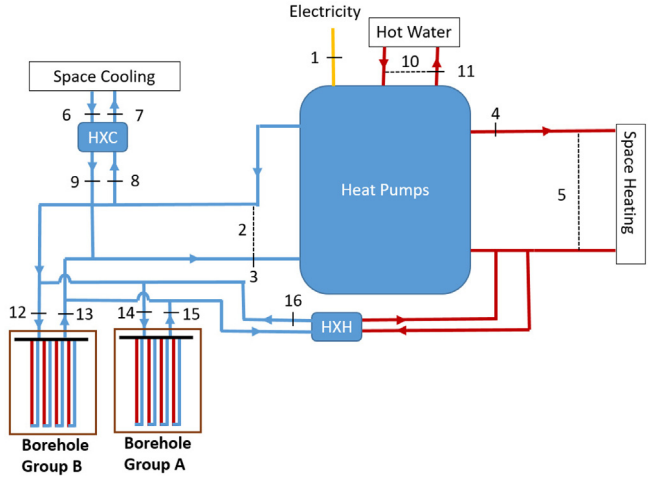

Fig. 4. Schematic of measurements of the GSHP-system.

pump is presented in section 3.2, and section 3.3 describes the model for the heat exchanger HXC based on an LMTD approach. The procedure to combine the individual models into a system model is described in section 3.4. The method to optimize the operation of the GSHP using the system model is described in section 3.5.

3.1. BHE model

The model for the BHE is based on the hybrid analytical ANN model presented by the authors in [60]. The model uses an analytical model with a time resolution of 1 day as an input to an ANN model, which predicts the heat injected/extracted into/from the ground by each borehole group with a time resolution of 1 h. The inputs of the ANN model used to predict the power of the borehole at time step t to t+1 are represented in Fig. 5. A detailed description of the model and comparison of the model's performance compared to other models is available in [60].

The model used in this study has a few minor changes compared to the one presented in [60]. In [60], an ensemble of 15 networks was used to improve the model's accuracy. However, in this study, we decided to use a single network instead of the ensemble as the increase in accuracy of the model was not sufficient to justify the additional computational time required to run 15 ANN networks. The input vectors, containing all 37 inputs of the ANN model were randomly sorted into training and validation sets. 80% of the input vectors were sorted into the training set and the other 20% was sorted into the validation set.

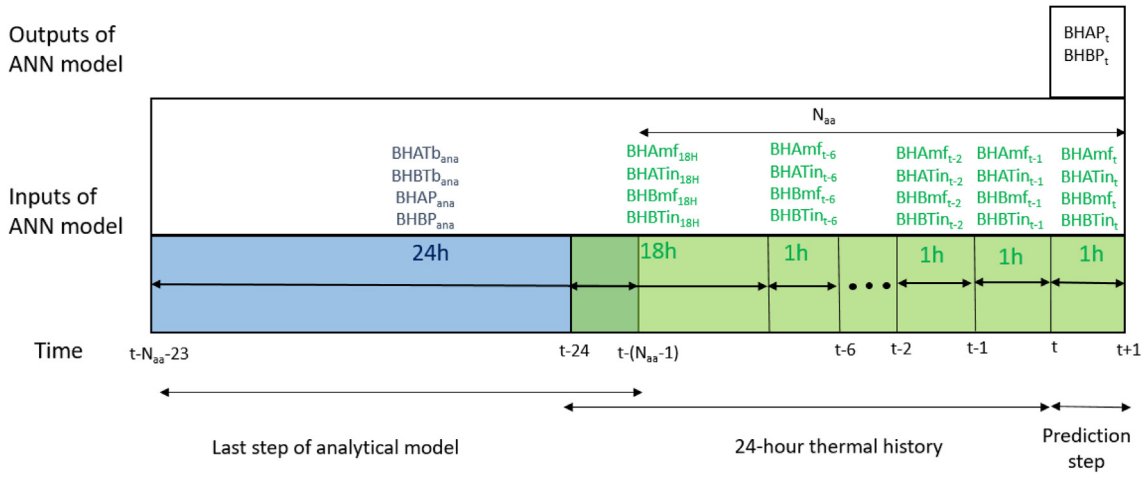

Fig. 5. Inputs and output of ANN model of BHE represented on a timeline (adapted from [60]).

3.2. Heat pump model

The GSHP system has three heat pumps; a detailed description of the heat pumps and their models were presented in [61]. ANN models were compared with regression models in [61]. However, in this study, we used one ANN to model the combined output from all three heat pumps, which reduces the complexity of the model. The value of interest is the total power of the compressors (CompPower), which was chosen as one of the two outputs of the ANN model. Even though the heat pump consists of on/off compressors. The compressor power is assumed a continuous variable since there are 10 compressors in the GSHP and we are using a relatively low time resolution of 1 h. The power of the compressors determines the mass flow rates in the heating and cooling circuit. Hence, the rate of mass flow on the cooling side, HPCoolmf, was chosen as the other output of the ANN model.

We developed two models for the heat pump, one for heating mode and the other for cooling mode. The inputs of the heat pump model for the heating mode are heat produced by the heat pump (HPHeatPower), HPHeatTout, DHWPower, DWHTout, HPCoolTin, and mode number. Mode number is a number used to represent the mode of the GSHP. In heating mode, HPHeatPower is equal to the sum of BY10Power and BY23Power. The heat pump model for the cooling mode uses HPCoolPower as the input instead of HPHeat power.

The non-faulty measured data were randomly divided into training, validation, and testing sets. 70% of the data was used for training, 15% for validation, and 15% for testing. The number of hidden nodes was chosen by increasing the number of nodes until the validation error increased with an increase in the number of hidden nodes. ANN architectures with 1 and 2 hidden layers were tried.

3.3. Heat exchanger model

HXC is a counter flow plate heat exchanger, with the cooling circuit of the heat pump on one side and the cooling circuit of the building on the other. The following equations give the heat transfer in the heat exchanger.

$$CoolPower = U \times A \times LMTD \tag{1}$$

$$CoolPower = Coolmf \times CoolCp \times (CoolTout - CoolTin) \tag{2}$$

$$CoolPower = BYCoolmf \times BYCoolCp \times (BYCoolTin - BYCoolTout) \tag{3}$$

where, CoolPower is the cooling demand of the building, U is the overall heat transfer coefficient of the heat exchanger, A is the effective area of the heat exchanger, LMTD is the log mean temperature difference given by equation (4), Coolmf and BYCoolmf are the mass flow rates on the heat pump side building side respectively. CoolPower is positive when heat is transferred from the building to the cooling circuit of the heat pump.

$$LMTD = \frac{(BYCoolTin - CoolTout) - (BYCoolTout - CoolTin)}{\ln(\frac{BYCoolTin - CoolTout}{BYCoolTout - CoolTin})} \tag{4}$$

The overall heat transfer coefficient U depends on the mass flow rates, Coolmf and ByCoolmf. The dependence of U × A on Coolmf and ByCoolmf can be approximated by equation (5). Equation (5) was derived based on the empirical expression in [64].

$$U \times A = \frac{1}{\frac{a}{BYCoolmf^{0.8289}} + \frac{b}{Coolmf^{0.8289}} + c} \tag{5}$$

The coefficients a, b and c were calculated by fitting equation (5) to the measured value.

The values of CoolPower, BYCoolTin, and BYCoolTout can be obtained from the cooling demand of the building. BYCoolmf was calculated using equation (3). In the cooling mode, Coolmf was obtained from the heat pump model, and CoolTout and CoolTin were calculated using equations (1) and (2). While in the heating mode, CoolTin was obtained from the heat pump model, and CoolTout and Coolmf were calculated from equations (1) and (2).

3.4. System model

The BHE, the heat pump, and the heat exchanger models were used to make a model for the whole GSHP system. Fig. 6 shows the main steps of the system model. The model's inputs are heating and cooling loads of the building, the temperature requirements and the thermal history of the BHE before the start of the simulation period.

The model uses the inputs to calculate the state of the GSHP at each time step. The model assumes a balance of power in the heating and cooling circuits at each 1-hour time step. In the heating modes, the borehole groups A and B are connected to the cooling circuit. In the free cooling with active cooling mode, borehole group A is connected to the heating circuit while borehole group B is connected to the cooling circuit. In active cooling mode, both the borehole groups are connected to the heating circuit. Therefore, three different models were created for the three configurations based on power and mass balance. The models for the three config-

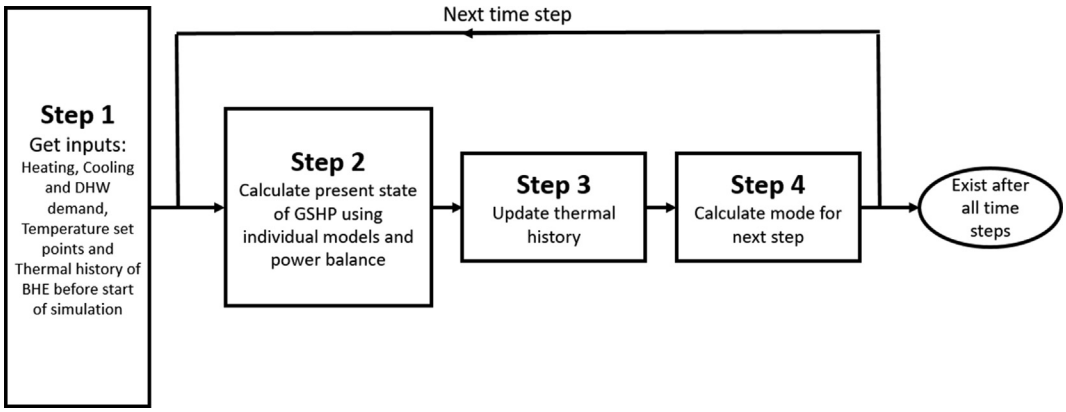

Fig. 6. Flow chart showing the steps of the system model.

urations are presented in sections 3.4.1–3.4.3. The power of the borehole calculated in step 2 is used to update the thermal history of the BHE. The thermal history is included in the hybrid BHE model using 24-hour thermal history and the outputs of the analytical model as shown in Fig. 5. The 24-hour thermal history is updated every hour. However the output of the analytical model is updated every after every 24 h since the analytical model has a time step of 24 h. The mode of the system for the next time step is then estimated based on the state of the system in the current time step as described in section 3.4.4.

3.4.1. Heating

In heating mode, the heat pump operates to satisfy the heating demand. The inlet temperature of the cool side of the heat pump (HPCoolTin) is determined from the power balance for the cold circuit using an iterative process, as shown in Fig. 7. The heat pump model outputs HPCoolmf and CompPower. Outlet temperature from the cool side of the heat pump (CoolTin) is then calculated using equations (6) and (7).

$$HPCoolPower = HPHeatPower - CompPower \tag{6}$$

$$CooTin = HPCoolTin - \frac{HPCoolPower}{HPCoolmf \times Cp} \tag{7}$$

Coolmf and CoolTout are then calculated using the heat exchanger model of section 3.3. The inlet temperature and the mass flow rate of the BHE depend on the mode of the GSHP. For heating with BHE in parallel to HXC mode, the inlet temperature (BHTin) and mass flow rate (BHmf) are:

$$BHTin = CoolTin \tag{8}$$

$$BHmf = HPCoolmf - Coolmf \tag{9}$$

For heating with BHE in series to HXC, the inlet temperature (BHTin) and mass flow rate (BHmf) are:

$$BHTin = Coolmf \times CoolTout + (HPCoolmf - Coolmf) \times CoolTin \tag{10}$$

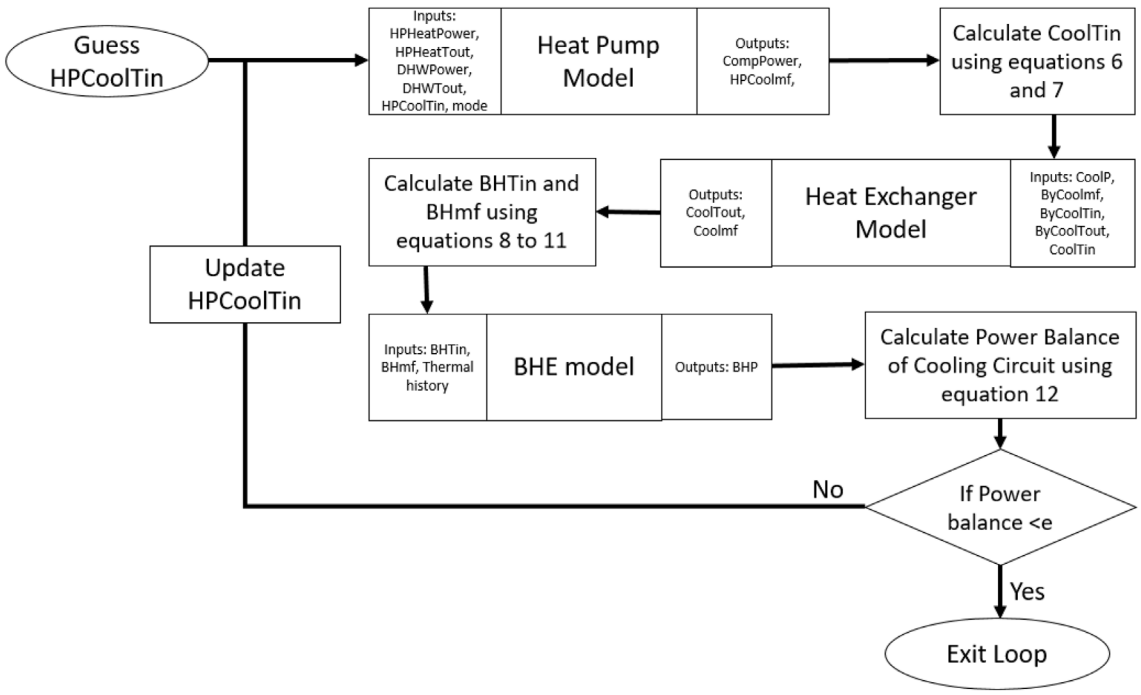

Fig. 7. Flow chart for GSHP in heating mode.

$$BHmf = HPCoolmf \tag{11}$$

The BHE model is run with the above inputs to obtain the power injected/extracted from the BHE. The power balance of the cooling circuit (PowerBalanceCC) is then calculated according to equation (12).

$$PowerBalanceCC = HPCoolPower - CoolPower - BHAP - BHBP \tag{12}$$

HPCoolTin value is updated to minimize PowerBalanceCC until PowerBlanceCC reaches a specified value e.

3.4.2. Free cooling with active cooling

In free cooling with active cooling mode, the cooling load determines the power supplied by the heat pump. However, the cooling from the heat pump (HPCoolPower) is lower than cooling load (CoolPower) since free cooling satisfies a part of the cooling demand. Therefore, both HPCoolPower and HPCoolTin are unknown and must be iteratively determined, by the procedure shown in Fig. 8.

In cooling mode, HPCoolPower is adjusted to obtain the necessary temperature at BYCoolTout. The model represents this by adjusting HPCoolPower was adjusted to obtain the required CoolTin (CoolTinReq). The difference between CoolTinReq, obtained using the heat exchanger model, and CoolTin from the heat pump is minimized iteratively.

$$DCoolTin = CoolTin - CoolTinReq \tag{13}$$

The inlet temperature and mass flow rate of borehole group B are CoolTout and HPCoolmf, respectively. Borehole group A is connected to HXH. The excess heat from the heat pump is injected into borehole group A, hence BHAP is calculated from the power balance equation of the heating circuit. BHATin is maintained at the temperature set by the external controller. BHAmf and BHBP are calculated using the BHE model with the above inputs. Finally, the power balance of the cooling circuit is calculated according to equation (14).

$$PowerBalanceCC = HPCoolPower - CoolPower - BHBP \tag{14}$$

HPCoolTin and HPCoolPower are adjusted to minimize.

$$PowerBalanceCC + f \times DCoolTin \tag{15}$$

where f, is a weight factor chosen to equal importance to PowerBalanceCC and DCoolTin.

3.4.3. Active cooling

In active cooling mode, the total cooling power is provided by the heat pump. Therefore, only HPCoolTin needs to be iteratively determined, as shown in Fig. 9. CompPower and HPCoolmf are determined from the heat pump model. CoolTin and CoolTinReq are calculated using equations (1), 2, 6, and 7, using the same procedure as free cooling with active cooling mode. HPCoolTin is then updated to minimize DCoolTin.

Both the borehole groups are connected to HXH in active cooling. The total borehole power is calculated from the power balance equation of the heating circuit and the inlet temperature of the BHE is a set temperature. The mass flow rate of borehole group A (BHAmf) is also fixed at maximum pump speed, while the mass flow rate of borehole group B (BHBmf) is controlled such that the combined power of the two boreholes is equal to the excess heat from the heat pump. The BHE model is used to calculate the distribution of borehole power (BHP) between the borehole groups and BHBmf.

3.4.4. Selection of mode

The mode of the GSHP is selected based on the state of the GSHP in the previous time step. The mode of the GSHP is changed from heating with BHE in parallel to HXC to active cooling as the cooling load increased and vice versa as the heating load increases, similar to the actual operation. The criteria for changing the mode were selected to simulate the real operation, as shown in Fig. 10. In actual operation, the mode switches from heating with BHE in parallel to HXC to heating with BHE in series to HXC if the cooling load increases and the valve opens beyond a threshold value. In the simulation, the mode is changed when the ratio of CoolPower to HPCoolPower is over a threshold value, SP1. Similarly, the mode changes from heating with BHE in series to HXC to heating with BHE in parallel to HXC when the ratio of CoolPower to HPCoolPower is below a threshold value SP3. The threshold values SP1 and SP3 were selected to minimize the misclassification of the mode for the measured values. The mode changes from heating with BHE in series to HXC to free cooling with active cooling mode when the heat pump cannot provide sufficient cooling; hence the cooling load controls the heat pump. This is represented in the simulation when the HPCoolPower is not sufficient, and hence the power balance in the cooling circuit cannot be satisfied. The change in mode from free cooling with active cooling to heating with BHE in series to HXC occurs when excess heat is not required to satisfy the cooling demand, i.e., when ExcessHeat is zero. The active cool-

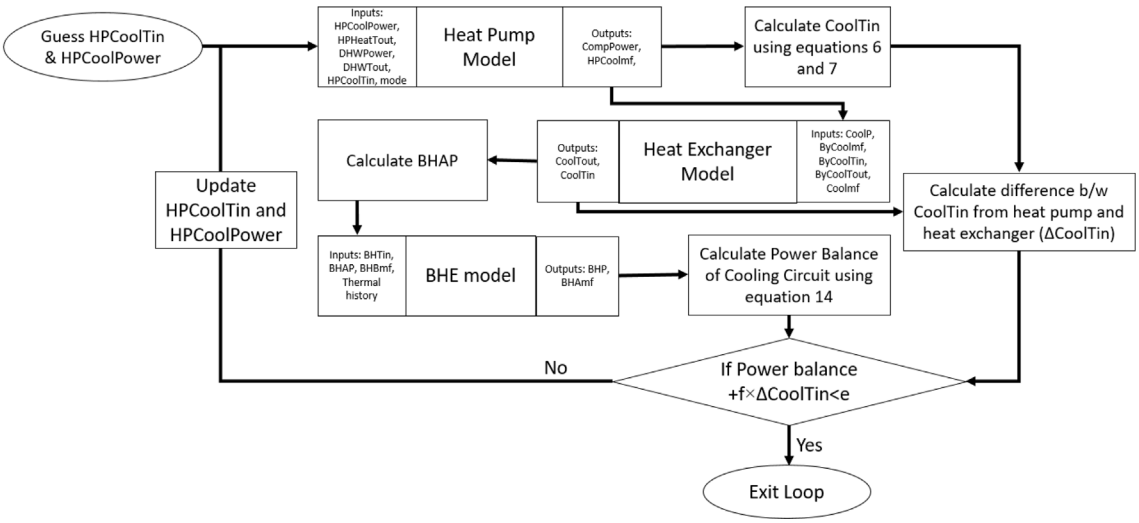

Fig. 8. Flow chart for GSHP in free cooling with active cooling mode.

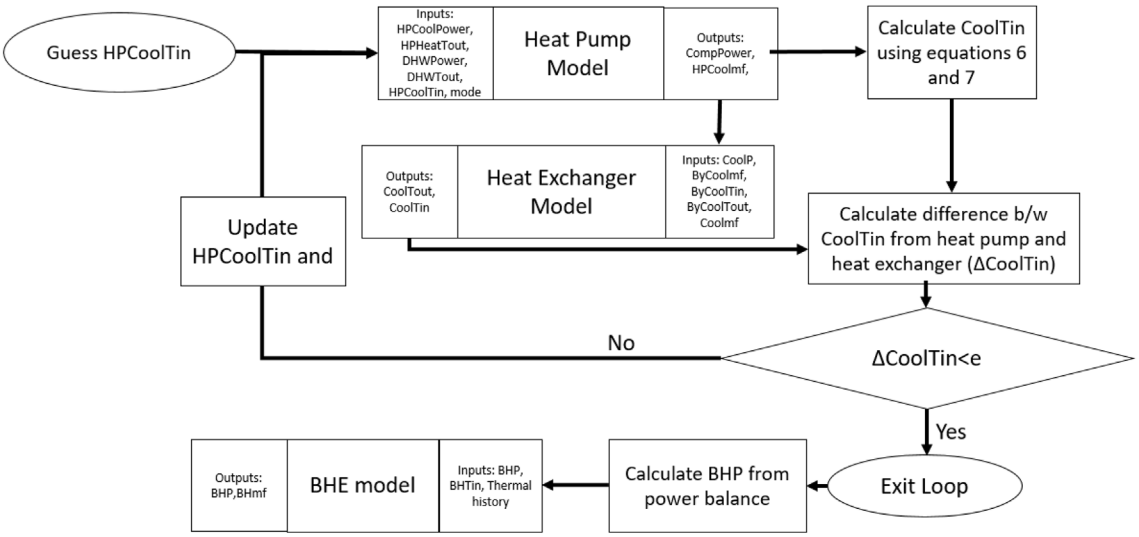

Fig. 9. Flow chart for GSHP in active cooling mode.

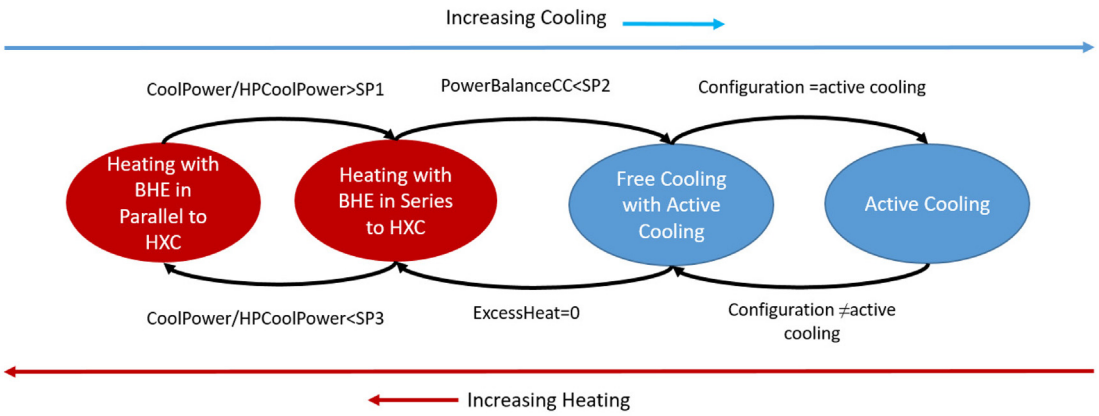

Fig. 10. Criteria for selection of mode.

ing mode was selected manually in the simulation since the operator selected the active cooling mode manually for a few days of the year manually after July 2019.

3.5. Operation optimization

The operation of the GSHP system was improved using the validated model. The operation of the GSHP system was improved by changing the heating and cooling load distribution between the GSHP-system and the DHC network. The main constraint in this study is to have a balanced operation of the BHE to ensure a sustainable operation of the GSHP system. The objective of the study is to reduce the yearly operation cost from the point of view of the energy company (Umeå Energi AB).

The cost was reduced by maximizing the utilization of the cheapest source of heating/cooling at every time step while ensuring a balanced operation of the BHE. To ensure long-term a balanced operation of the BHE, a penalty variable ϵ was used to modify the threshold for choosing the heat source. We defined two modes of operation for the GSHP, base, and max. The GSHP is considered to be operating in the base mode when an increase in the power of the heat pump (CompPower) results in an increase in both CoolPower and SHPower. In the cooling mode, the GSHP is in base mode if the ExcessHeat is zero, and in the heating mode, the GSHP is in base mode if BHAP and BHBP are greater than zero. The GSHP is considered to be in max mode if the GSHP is operating at maximum power or if the GSHP meets both the heating and the cooling demand of the building.

The cheapest source of heating/cooling is determined by comparing the variable cost of producing the marginal district heating or cooling with the variable of electricity that will be used by the GSHP to replace the district heating or cooling. In the max mode, the marginal CompPower is used to substitute district heating in the heating mode and district cooling in the cooling mode. Therefore, the GSHP is operated in max mode if the inequality 16 or 17 are satisfied; else, the GSHP is operated in base mode. The penalty variable ϵ was selected by trial and error until the difference between the average borehole wall temperature of the first year and the last year for the 50 year simulation was less than 1 °C.

$$\text{In heating mode} \frac{Marginal\ cost\ of\ elecrticity}{COP_{Heat}} + \epsilon < Marginal\ cost\ of\ district\ heating \quad (16)$$

$$\text{In cooling mode} \frac{Marginal\ cost\ of\ elecrticity}{COP_{Cool}} - \epsilon < Marginal\ cost\ of\ district\ cooling \quad (17)$$

where,

$$COP_{Heat} = \frac{SHPower}{CompPower} \quad (18)$$

$$COP_{Cool} = \frac{CoolPower}{CompPower} \quad (19)$$

The marginal electricity comes from the regional grid since the company does not generate the majority of its electricity. The marginal district heating and cooling is supplied by the unit with the lowest priority among the different units operating at a particular time.

The energy company provided the variable operating cost of each facility for district heating and cooling. The energy company also provided the information on the facility with the least priority operating at each hour for 4 years. Table 3 shows the variable operating cost, CO_2 emissions, and the fuel of each facility in the order of priority assigned by the energy company. The cost includes the fuel cost and the taxes associated with it. The distribution loss of district heating and cooling was included by multiplying the cost by a loss factor (see Fig. 11). The size of the loss factor depends mainly on the load and its variation over the year and the outdoor temperature. Therefore, different loss factors are used for each month of the year based on the losses reported by the energy company. The marginal cost of electricity was calculated as the hourly spot price of electricity for the regional grid, [65], plus transmission cost and taxes obtained from the energy provider. The marginal CO_2 emissions for electricity is considered as 350 kg/MWh.

The district heating and cooling demand of the hospital was obtained from the energy meters. The hospital consists of many buildings with different efficiencies. Some of the older buildings in the hospital require a higher supply temperature for heating. Hence the GSHP system cannot provide heating for such buildings. This study will only consider the district heating demands of the newer buildings which can be connected to the GSHP. This represents 30% of the total heating demand of the hospital.

The model is simulated for the next year, i.e., from May 2021 to April 2022. This implies that the BHE model considers that the temperature of the ground is in the present condition, i.e, May 2021. To evaluate the long term of the GSHP, we used a 50-year simulation of the BHE using only the low time resolution analytical model and not the hybrid model since the analytical model is sufficient to estimate the long-term response of the ground. We used the monthly average of the ground loads from the 1-year simulation of the GSHP system as the input to the analytical model. The change in the borehole wall temperature was used as a measure to evaluate the sustainability of the operation of the GSHP system.

The results of the simulation were compared with the existing scenario. The inputs for the existing scenario were calculated as the average of four years of measured data, i.e., the hourly inputs are calculated as the weighted average of the four years, with a zero weight for faulty measured data and one for the non-faulty measured data.

4. Results

The results of the individual models for the BHE, heat pumps, and heat exchanger are presented in section 4.1. The validation of the system, by comparing it with the field measurements is presented in section 4.2. Section 4.3 and 4.4 describe the results of modified operation of the GSHP system. The existing scenario, which will be used as a reference, is presented in Section 4.3. The improved scenario with a reduced cost and a balanced operation of BHE is presented in section 4.4.

4.1. Individual models

The deviation of the hybrid BHE model compared to the measured data is shown in Table 4. The model has a mean absolute error (MAE) of 15.91 kW, corresponding to a relative MAE of 4.24% (i.e., compared to the average absolute load). The error is similar to [60], which had a relative MAE of 3.54%.

Two models were developed for the heat pump, summer and winter. The measured data were divided into training, validation, and testing sets, with 70%, 15%, and 15% of the points, respectively. The number of nodes of each model was selected based on the validation error. A network with two hidden layers with 35 and 30 nodes in each layer was selected for the heating and cooling mode models, respectively. The deviation of the selected models is shown in Table 5.

The heat exchanger model was calibrated by fitting the coefficients of equation (5) using the measured data. Values of $U \times A$ were calculated from equation (20) by:

Table 3
Marginal variable production cost and CO_2 for heating and cooling production units in the district heating and cooling network.

Production unit	Fuel	Relative production cost	Relative CO_2 production	COP
District heating				
Boiler 1	Waste	1.00	1.00	
Boiler 2	Biomass	3.41	0.12	
Boiler 3	Biomass	3.02	0.12	
Heat Pump 1	Electricity	El	3.47	3.4
Boiler 4	Biomass	5.32	0.12	
Heat pump 2	Electricity	El	3.47	3.4
Heat pump 3	Electricity	El	3.47	3.5
Boiler 5	Biomass	5.80	0.12	
Electric heater 1	Electricity	El	3.47	
Electric Heater 2	Electricity	El	3.47	
Boiler 6	Oil	21.59	2.88	
Boiler 7	Bio-Oil	15.18	0.59	
Boiler 8	Oil	20.75	2.88	
Boiler 9	Oil	20.75	2.88	
Boiler 10	Oil	21.29	2.88	
District Cooling				
Free Cooling Air		0	0	
Free Cooling river		0	0	
Absorption cooler	District heating	DH	DH	0.7
Compression cooler 1	Electricity	El	3.47	2.75
Compression cooler 2	Electricity	El	3.47	3.25
Compression cooler 3	Electricity	El	3.47	3.25

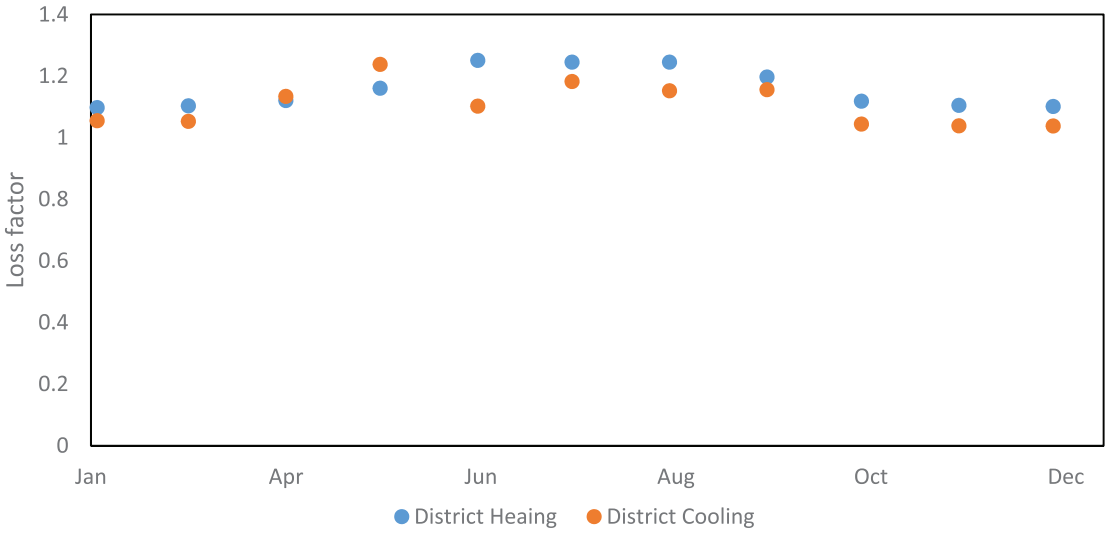

Fig. 11. Loss factor for different months of the year.

Table 4
Deviation of the BHE model.

MAE (kW)	% error	MAE (kW)	% error	MAE (kW)	% error
15.9	4.2	15.6	4.2	17.0	4.6

$$U \times A = \frac{CoolPower}{LMTD} \tag{20}$$

The log mean temperature difference (LMTD) was calculated from the measured temperatures, using equation (4). CoolPower was calculated from the power balance of the cooling circuit of the heat pump. The power balance equation depends on the mode of the GSHP. Equations 21–23 shows the power balance equations for different modes.

$$\text{For Heating } HPCoolPower = CoolPower + BHAP + BHBP \tag{21}$$

$$\text{For Free Cooling with Active Cooling } HPCoolPower = CoolPower + BHBP \tag{22}$$

$$\text{For Active Cooling} HPCoolPower = CoolPower \tag{23}$$

The measured values for BYCoolmf and Coolmf were calculated from equations (3) and (2), respectively. The R^2 of the fit for U × A was 0.8721, and the MAE of the fit was 32.86 kW/°C, which is 17.6% of the average value of U × A.

4.2. Validation of system model

The GSHP model was validated using the measured data from May 2017 to April 2021. The heating and cooling demand of the building and the required temperatures were the inputs to the model. The MAE for CompPower is 14.85 kW, which is 7.3% of the average CompPower. Fig. 12 shows the moving average of deviation between the measured and simulated values of CompPower and the moving average of the measured CompPower. The figure shows that the predicted CompPower has a good agreement with the measured CompPower. The average simulated CompPower is 3.2 kW lower than the measured value. The error is higher for cooling mode compared to heating mode. The relative MAE is 12.0% in cooling mode compared to 5.8% in heating mode. The simulation had a run time of about 9 h on a standard computer with 16 GB RAM and a 3.4 GHz Intel i7 processor.

Fig. 13 shows the moving average of the deviation between the measured and simulated power extracted by the BHE (BHP) and their absolute values. The MAE of the BHP is 71.3 kW, which is 19.1% of the mean absolute of BHP. The mean bias error is −47.0 kW, i.e., the simulation overestimates the heat injected into the ground. The relative MAE for heating and cooling mode is 14.0% and 23.8%, respectively. Fig. 13 shows that measured and simulated values of BHP have a good agreement. However, the MAE is 4.5 times higher than the MAE of the individual BHE model. Some of the reasons for the deviation are discussed in section 5.

4.3. Existing operation

The results of simulating the existing scenario of the GHSP system is presented in this section. In this scenario, the average CompPower is 195.6 kW (the compressor power at design condition is 300 kW. The hospital gets 45.6% of the heating load and 8.4% of

Table 5
Error of the selected heating and cooling mode models.

		Train		Validation		Test		Total	
		MAE (kW)	% error	MAE (kW)	% error	MAE (kW)	% error	MAE (kW)	% error
Winter	CompPower	7.5	3.7	7.8	3.8	7.5	3.7	7.6	3.7
	HPCoolmf	1.2	3.0	1.3	3.2	1.3	3.3	1.3	3.1
Summer	CompPower	8.8	4.3	8.7	4.3	8.8	4.3	8.8	4.3
	HPCoolmf	1.3	3.1	1.3	3.2	1.4	3.3	1.3	3.2

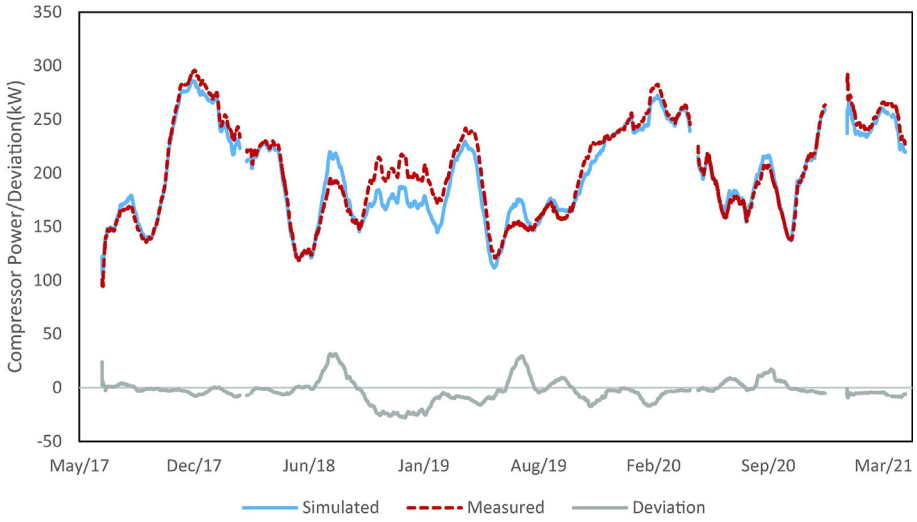

Fig. 12. Measured and simulated values of compressor power along with deviation.

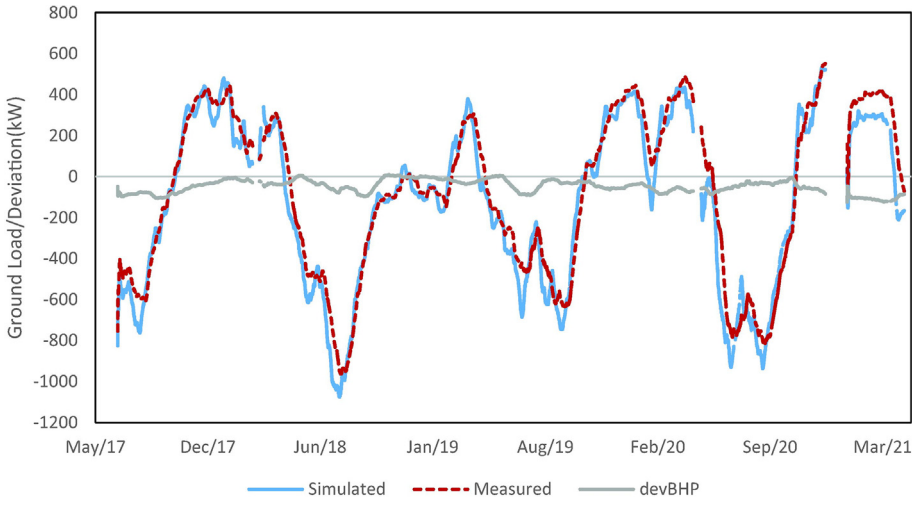

Fig. 13. Measured and simulated values of BHE load along with deviation.

the cooling load is from the DHC network. The moving average of the percentage of heating and cooling loads covered by the GSHP is shown in Fig. 14. As expected, the GSHP covers almost all of the cooling load in winter, and the percentage decreases in summer when the cooling load is too high for the GSHP to cover the entire load. Similarly, the GSHP covers a majority of the heating load in summer and a smaller part in winter.

In the existing scenario, the total marginal cost is 322 t€ and the total marginal CO_2 emissions is 1220 tons per year. The annual imbalance in the ground load is −0.99 GWh, i.e., 0.99 GWh of energy is injected into the ground every year. Fig. 15 shows the borehole wall temperature of the two borehole groups from the start of the modeled operation during 50 years. The borehole wall temperature will increase over the years. An increase in ground temperature will reduce the ability of the BHE to inject heat into the ground; hence the present scenario is not a sustainable way to operate the GSHP. This has already been observed in practice during the last few years. The operation of the GSHP has been modified since the ability of the GSHP to operate in free cooling with active cooling mode was observed to reduce over the years. Based on the simulation, the average borehole wall temperature was estimated to increase by 12 °C in 50 years compared to the initial temperature during the first year of operation.

4.4. Improved operation

The operation cost of the GSHP can be minimized in the short-term by setting the penalty variable (**ϵ**) as zero. However, this is not sustainable in the long term as the temperature of the ground will decrease over time, as shown in Fig. 16. Therefore, to make the operation of the GSHP system sustainable, we must reduce the threshold for the GSHP to be in max mode in cooling mode and increase the threshold in the heating season. We did this by choosing positive numbers for **ϵ**.

The value of **ϵ** was adjusted until the change in average borehole wall temperature between the first year of operation and 50 years from now was less than 1 °C. Fig. 16 shows the variation of annual marginal cost and the change in Tb during 50 years with **ϵ**. The change in borehole wall temperature (Tb) was less than 1 °C for a value of 7.5 €/MWh. Hence, **ϵ** was chosen to be 7.5 €/MWh. The annual marginal cost is 257 t€ for this case.

Fig. 17 shows the 30-day moving average of the percentage of heating and cooling load covered by the GSHP system. The GSHP system covers 69.6 % of the total annual heating demand and 96.8% of the cooling demand. The GSHP operates in the max mode for 68.1% of the time, resulting in an average CompPower of 232.1 kW.

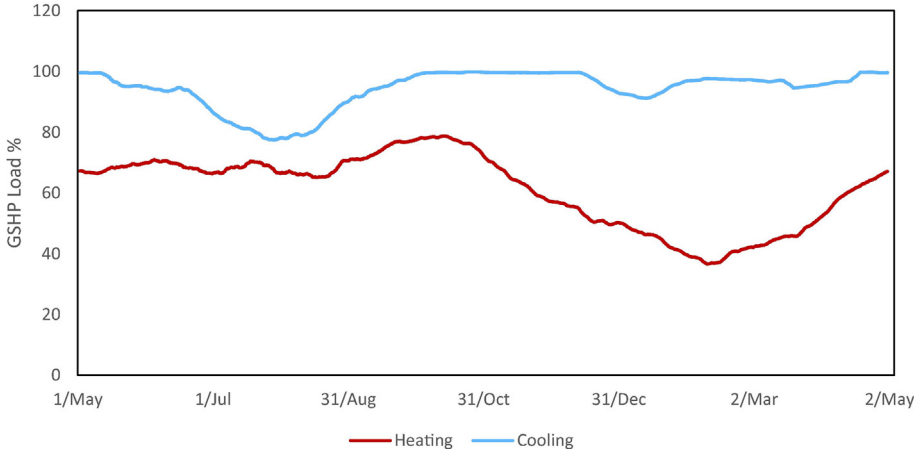

Fig. 14. Percentage of demand covered by GSHP in the present case.

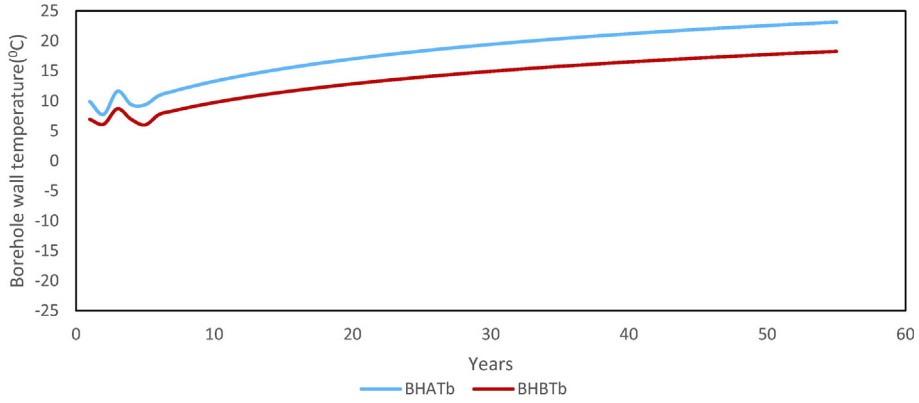

Fig. 15. Change in borehole wall temperature for the next 50 years for the present case.

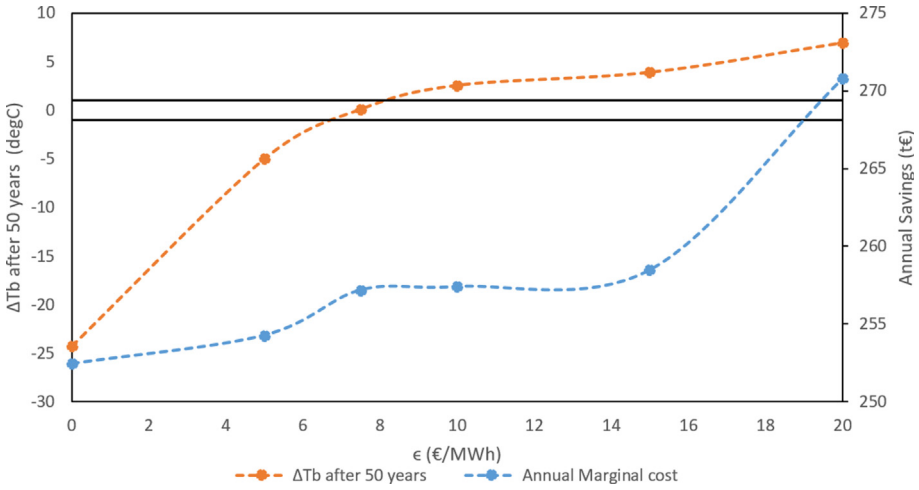

Fig. 16. Variation of change in borehole wall temperature and annual cost for different values of ϵ.

Fig. 18 shows that the annual average temperature of the ground is stable throughout the lifetime of the GSHP-system. Hence, the system can be operated in the improved scenario throughout the lifetime of the GSHP. The annual marginal cost is 257 t€, and the annual marginal CO_2 is 1128 tons for the improved scenario. Therefore, the annual cost of heating and cooling the buildings will reduce by 64 t€, and the annual CO_2 produced will reduce by 92 tons.

Table 6 shows a summary of results from the improved scenario and compares it with the existing scenario. The percentage of annual heating covered by the GSHP system increases from 54% to 70% in the improved operation case. The annual cooling covered by the GSHP increased slightly from 92% to 97%.

From the BHE energy balance we see that in the current scenario the heat extracted from the ground the higher than the heat injected, even though the operational cost can be reduced by

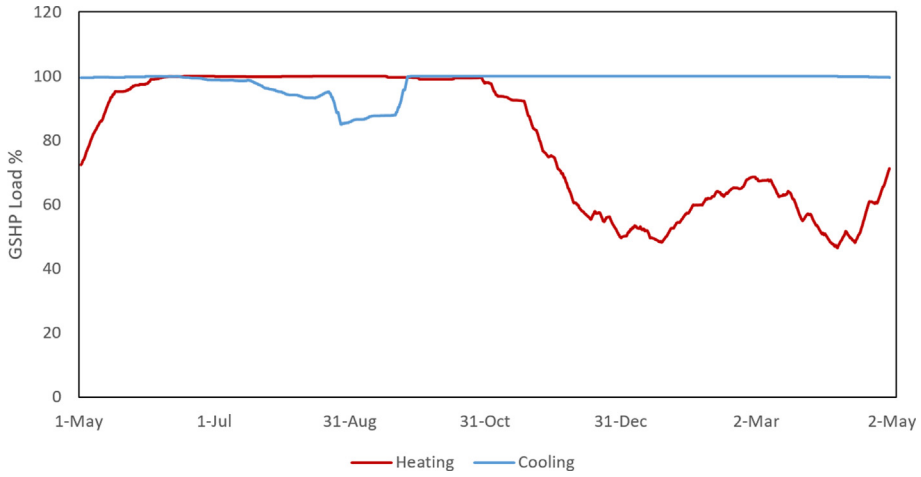

Fig. 17. Percentage of demand covered by GSHP in the optimal case.

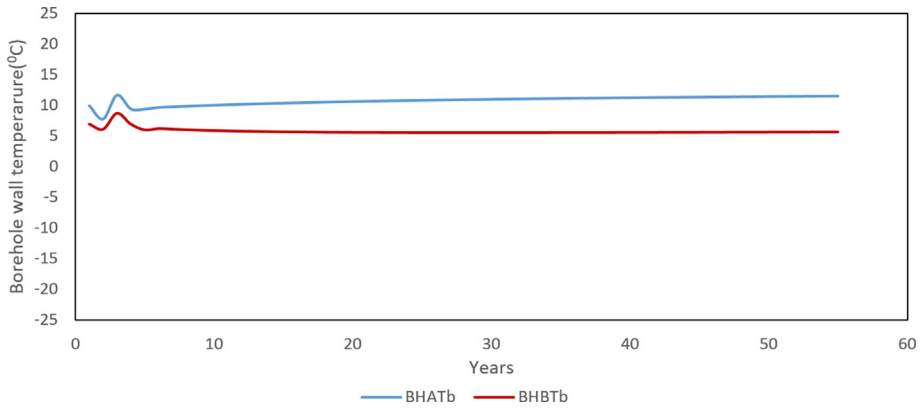

Fig. 18. Change in borehole wall temperature for the next 50 years for the optimal case.

increasing the use of GSHP. This highlights the need for modeling of existing GSHP systems. A good model can be used to make the operational strategy of a GSHP system more sustainable and economical.

Table 6
Comparison of results from different operation scenarios.

		Existing Operation	Improved Operation
Annual Heating	GSHP (GWh)	5.0	6.4
	DH (GWh)	4.2	2.8
	% covered by GSHP	54%	70%
Annual cooling	GSHP (GWh)	4.3	4.5
	DH (GWh)	0.4	0.1
	% covered by GSHP	92%	97%
GSHP Electricity (GWh)		1.7	2.0
BHE balance	Yearly imbalance (GWh)	−1.0	−0.1
	50 year temperature change (°C)	12	0.15
Annual Marginal Cost	Electricity (t€)	126	150
	DH (t€)	189	105
	DC (t€)	8	3
	Total (t€)	322	257
Annual Marginal CO_2	Electricity (tons)	600	712
	DH (tons)	614	416
	DC (tons)	6.8	0
	Total (tons)	1221	1128

5. Discussion

This study demonstrates that accurate models of components of a heating system can be developed using measured data. Section 4.1 shows that MAE of 4.2% can be achieved using the hybrid model for BHE and that the ANN model of the combined heat pumps can accurately predict both the power (MAE 3.8%) and flow rate (MAE 3.1%) in the heat pump. The models developed are not only accurate but also simple enough to be used as components in a complex system.

The borehole heat exchanger, heat pump, and heat exchanger models were used to represent the operation of a GSHP that has been monitored for four years. The system model was validated using four years of measured data. Section 4.2 presents the results of the validation. The simulation represents the actual performance accurately with a reasonable computational time. The MAE for CompPower was 7.8%, and the MAE for the power of the BHE was 19.1% and the computational time for simulating 4-year operation was approximately 9 h.

Although the error in CompPower is low, the error in the power of the BHE is considerably higher than the error of the individual BHE Model. This implies that the deviation is due to the error in calculating the inputs of the BHE model. One of the sources of error is the heat exchanger model, and the fitted U × A value has an MAE of 17.6%. The heat exchanger model is used to calculate the CoolT-out, which affects the inlet temperature of the boreholes. The inlet temperature of the boreholes also depends on the mode of the

GSHP. Hence an error in recognizing the mode of the GSHP will affect the performance of the BHE model. The mode determined from the measured data does not match the simulated mode for 16.4% of the points. The MAE for these points is 100.1 kW compared to 65.7 kW for the rest of the points, which implies that an erroneous mode selection increases the deviation in BHP.

The model assumes that no heat is stored in the working fluid, due to which the transient behavior of the GSHP cannot be fully captured by the model. The error of the daily average of values of BHP is approximately 14%, which is less than the hourly values. The model also assumes that the control of the GSHP is perfect. However, there can be a significant difference between the control objectives and the actual system. This was observed in the control of the circulation pumps for the BHE. The control system aims to prevent bypass flow in BP. However, from the measurements, we see that there is significant flow in BP, especially in free cooling with active cooling mode. The model also assumes that there are no heat losses in the GSHP system, which is not true in practice. The effect of heat losses was observed to be significant in HXH as the measured power at HXH was different from the heat injected into the ground.

Another source of error is faults in the actual system due to malfunctioning components or measurement systems. The authors detected some of the faults in the system using the measurements. However, exhaustive fault detection was not performed, as it was not in the scope of this study. Additionally at every time step HPCoolTin (and HPCoolPower) are calculated iteratively, by minimizing the residual of the power balance equation, using a nonlinear optimization algorithm *(Nelder-Mead simplex algorithm)*. The minimization does not always find good minima. The residual of the power balance equation was greater than 100 kW for around 6.9% of the points.

The explanation above provides some of the possible reasons for the error in simulated BHP. As a consequence of the error, the average deviation between simulated and measured data is −47 kW. A deviation of −47KW in ground load could result in an error of 6 °C while calculating the borehole wall temperature after 50 years, which is one of the criteria for selecting the improved operation of BHE. Therefore, the borehole heat exchanger might have some imbalance even in the improved operation. Hence reducing the deviation will increase the confidence in the proposed operational scheme. Some ways to reduce the deviation, like improving the heat exchanger model, alternative ways to define the thresholds for changing the mode, and including heat losses in the model, can be explored in future work. The models can also be improved by retaining the models as more data becomes available. The uncertainty in the measured data can also be reduced by including more measurements, like the mode of operation, bypass flow of the BHE, flow through HXC, etc. Additionally, usage of faulty data for training and evaluation of the model can be reduced using by maintaining a better record of faults in the system.

The validated model was used to improve the operation of the GSHP system. In particular, the distribution of heating and cooling from the GSHP and the district heating and cooling network was improved. We showed that using the present operation scenario would increase the borehole wall temperature over time. Therefore, the power injected into the ground will decrease over time. Hence, the preset operation scenario is not sustainable in the long term. Section 4.4 shows that minimizing the annual cost of the operation in the short term will decrease the borehole wall temperature over time, and the BHE will not be able to extract the same amount of heat in the future. Therefore, the improved scenario presented in section 4.4 uses a penalty variable to ensure a balanced operation of the borehole heat exchanger. In the improved scenario the annual operation cost will reduce by 64 t€ and the CO_2 emission will reduce by 92 tons with negligible change in temperature at the borehole wall over the years. The method to arrive at the improved scenario described in section 3.5 can be generalized to any GSHP.

In this study, we reduced the cost of production of energy for the energy company. However, the operation of the GSHP is handled by the building manager at the hospital. This contradiction highlights the need for better cooperation between the building managers and the energy utility companies. The results of the study show that both reductions of operational cost and stable long-term operation of the GSHP can be achieved through such cooperation. However, for the cooperation to be successful, the benefits of the change in operation should be shared between the energy utility company and the building manager through innovative cost/business models.

6. Conclusion

An ideal operation of a GSHP system should reduce operating costs and ensure that the performance of the BHE does not deteriorate over the long term. The lack of a reliable method to predict short-term and long-term performance is a limitation for improving the operation of GSHP systems. This study addressed that challenge by using measured data to develop models that are both accurate and simple. We used a hybrid analytical-ANN model for the BHE, an ANN model for the heat pumps, and an empirical model for the heat exchangers. The BHE model and the heat pump models were demonstrated to be accurate, with an MAE of less than 5%, while the heat exchanger model has an MAE of 17.6%.

The actual operation of a GSHP installation was simulated using the models. The model of the GSHP system was validated using four years of monitored data. The model had good agreement with the measured data, the simulated compressor power had an MAE of 7.8% and the simulated power of the borehole had an MAE of 19.1%. The validated model was used to improve the operation of the GSHP system, the annual cost of the energy company for providing heating and cooling to the building was reduced while ensuring a sustainable long-term operation. We showed that a stable long-term operation can be achieved while reducing the annual operation cost by 64 t€. The annual CO_2 emission can be reduced by 92 tons for this scenario.

Declaration of Competing Interest

The authors declare that they have no known competing financial interests or personal relationships that could have appeared to influence the work reported in this paper.

Acknowledgments

We would like to thank Region Västerbotten for providing the field measurements from the heating system at Norrland's university hospital and Umeå Energi AB for providing the data about district heating and cooling.

We would like to thank Industrial Doctoral School at Umeå University and Umeå Energi AB for their financial support

References

[1] E. Commission, An EU Strategy on Heating and Cooling, COM (2016) 51 Final, Belgium, Brussels, 2016.

[2] D. Connolly, H. Lund, B.V. Mathiesen, S. Werner, B. Möller, U. Persson, T. Boermans, D. Trier, P.A. Østergaard, S. Nielsen, Heat Roadmap Europe: Combining district heating with heat savings to decarbonise the EU energy system, Energy Policy 65 (2014) 475–489.

[3] A. David, B.V. Mathiesen, H. Averfalk, S. Werner, H. Lund, Heat roadmap Europe: large-scale electric heat pumps in district heating systems, Energies 10 (2017) 578.

[4] M. Åberg, L. Fälting, D. Lingfors, A.M. Nilsson, A. Forssell, Do ground source heat pumps challenge the dominant position of district heating in the Swedish heating market?, J Clean. Prod. 254 (2020) 120070.
[5] H. Averfalk, P. Ingvarsson, U. Persson, M. Gong, S. Werner, Large heat pumps in Swedish district heating systems, Renew. Sustain. Energy Rev. 79 (2017) 1275–1284.
[6] N.L. Truong, L. Gustavsson, Costs and primary energy use of heating new residential areas with district heat or electric heat pumps, Energy Procedia 158 (2019) 2031–2038.
[7] S. Gehlin, O. Andersson, J.-E. Rosberg, Country Update for Sweden 2020, in: Proceedings, World Geotherm. Congr. 2020, 2020.
[8] H. Lund, S. Werner, R. Wiltshire, S. Svendsen, J.E. Thorsen, F. Hvelplund, B.V. Mathiesen, 4th Generation District Heating (4GDH): integrating smart thermal grids into future sustainable energy systems, Energy 68 (2014) 1–11.
[9] B. Ciapała, M. Janowski, Geothermal power based ULTDH for cooling and heating purposes, in: E3S Web Conf., EDP Sciences, 2019: p. 9.
[10] G. Nouri, Y. Noorollahi, H. Yousefi, Solar assisted ground source heat pump systems–a review, Appl. Therm. Eng. 163 (2019) 114351.
[11] J. Huang, J. Fan, S. Furbo, Demonstration and optimization of a solar district heating system with ground source heat pumps, Sol. Energy. 202 (2020) 171–189.
[12] A.D. Carvalho, P. Moura, G.C. Vaz, A.T. de Almeida, Ground source heat pumps as high efficient solutions for building space conditioning and for integration in smart grids, Energy Convers. Manag. 103 (2015) 991–1007.
[13] K. Kontu, J. Vimpari, P. Penttinen, S. Junnila, Individual ground source heat pumps: Can district heating compete with real estate owners' return expectations?, Sustain Cities Soc. 53 (2020) 101982.
[14] W. Ma, S. Fang, G. Liu, Hybrid optimization method and seasonal operation strategy for distributed energy system integrating CCHP, photovoltaic and ground source heat pump, Energy. 141 (2017) 1439–1455.
[15] X. Zhang, H. Li, L. Liu, C. Bai, S. Wang, Q. Song, J. Zeng, X. Liu, G. Zhang, Optimization analysis of a novel combined heating and power system based on biomass partial gasification and ground source heat pump, Energy Convers. Manag. 163 (2018) 355–370.
[16] R. Zeng, H. Li, R. Jiang, L. Liu, G. Zhang, A novel multi-objective optimization method for CCHP–GSHP coupling systems, Energy Build. 112 (2016) 149–158.
[17] S. Miglani, K. Orehounig, J. Carmeliet, Integrating a thermal model of ground source heat pumps and solar regeneration within building energy system optimization, Appl. Energy 218 (2018) 78–94.
[18] S. Ikeda, W. Choi, R. Ooka, Optimization method for multiple heat source operation including ground source heat pump considering dynamic variation in ground temperature, Appl. Energy 193 (2017) 466–478.
[19] P. Eskilson, Superposition Borehole Model (SBM). Manual for Computer Code, (1986)
[20] H.Y. Zeng, N.R. Diao, Z.H. Fang, A finite line-source model for boreholes in geothermal heat exchangers, Heat Transf. Res. Co-sponsored by Soc. Chem. Eng. Japan Heat Transf. Div. ASME. 31 (2002) 558–567.
[21] L. Lamarche, B. Beauchamp, A new contribution to the finite line-source model for geothermal boreholes, Energy Build. 39 (2007) 188–198, https://doi.org/10.1016/j.enbuild.2006.06.003.
[22] L. Lamarche, A fast algorithm for the hourly simulations of ground-source heat pumps using arbitrary response factors, Renew. Energy 34 (2009) 2252–2258, https://doi.org/10.1016/j.renene.2009.02.010.
[23] M. Cimmino, M. Bernier, A semi-analytical method to generate g-functions for geothermal bore fields, Int. J. Heat Mass Transf. 70 (2014) 641–650, https://doi.org/10.1016/j.ijheatmasstransfer.2013.11.037.
[24] N. Molina-Giraldo, P. Blum, K. Zhu, P. Bayer, Z. Fang, A moving finite line source model to simulate borehole heat exchangers with groundwater advection, Int. J. Therm. Sci. 50 (2011) 2506–2513, https://doi.org/10.1016/j.ijthermalsci.2011.06.012.
[25] T.V. Bandos, Á. Montero, E. Fernández, J.L.G. Santander, J.M. Isidro, J. Pérez, P.J. F. de Córdoba, J.F. Urchueguía, Finite line-source model for borehole heat exchangers: effect of vertical temperature variations, Geothermics 38 (2009) 263–270, https://doi.org/10.1016/j.geothermics.2009.01.003.
[26] P. Monzó, Modelling and monitoring thermal response of the ground in borehole fields, Kungliga Tekniska högskolan (2018).
[27] C. Naldi, E. Zanchini, A new numerical method to determine isothermal g-functions of borehole heat exchanger fields, Geothermics 77 (2019) 278–287.
[28] A. Lazzarotto, A network-based methodology for the simulation of borehole heat storage systems, Renew. Energy 62 (2014) 265–275, https://doi.org/10.1016/j.renene.2013.07.020.
[29] L. Lamarche, Mixed arrangement of multiple input-output borehole systems, Appl. Therm. Eng. 124 (2017) 466–476, https://doi.org/10.1016/j.applthermaleng.2017.06.060.
[30] M. Cimmino, A finite line source simulation model for geothermal systems with series- and parallel-connected boreholes and independent fluid loops, J. Build. Perform. Simul. 11 (2018) 414–432, https://doi.org/10.1080/19401493.2017.1381993.
[31] B. Dusseault, P. Pasquier, D. Marcotte, A block matrix formulation for efficient g-function construction, Renew. Energy 121 (2018) 249–260.
[32] A. Zarrella, M. Scarpa, M. De Carli, Short time step analysis of vertical ground-coupled heat exchangers: the approach of CaRM, Renew. Energy 36 (2011) 2357–2367, https://doi.org/10.1016/j.renene.2011.01.032.
[33] D. Bauer, W. Heidemann, H. Müller-Steinhagen, H.-J.- G. Diersch, Thermal resistance and capacity models for borehole heat exchangers, Int. J. Energy Res. 35 (2011) 312–320, https://doi.org/10.1002/er.v35.410.1002/er.1689.
[34] S. Javed, J. Claesson, New analytical and numerical solutions for the short-term analysis of vertical ground heat exchangers, Ashrae Trans. 2011, Vol 117, Pt 1. 117 (2011) 3–12.
[35] M. De Rosa, F. Ruiz-Calvo, J.M. Corberán, C. Montagud, L.A. Tagliafico, A novel TRNSYS type for short-term borehole heat exchanger simulation: B2G model, Energy Convers. Manag. 100 (2015) 347–357, https://doi.org/10.1016/j.enconman.2015.05.021.
[36] M. Li, A.C.K. Lai, New temperature response functions (G functions) for pile and borehole ground heat exchangers based on composite-medium line-source theory, Energy. 38 (2012) 255–263, https://doi.org/10.1016/j.energy.2011.12.004.
[37] J. Wei, L. Wang, L. Jia, K. Zhu, N. Diao, A new analytical model for short-time response of vertical ground heat exchangers using equivalent diameter method, Energy Build. 119 (2016) 13–19, https://doi.org/10.1016/j.enbuild.2016.02.055.
[38] T.R. Young, Development, verification, and design analysis of the borehole fluid thermal mass model for approximating short term borehole thermal response, (2004).
[39] L. Lamarche, Short-time analysis of vertical boreholes, new analytic solutions and choice of equivalent radius, Int. J. Heat Mass Transf. 91 (2015) 800–807, https://doi.org/10.1016/j.ijheatmasstransfer.2015.07.135.
[40] J.M. Rivero, M. Hermanns, Enhanced multipole method for the transient thermal response of slender geothermal boreholes, Int. J. Therm. Sci. 164 (2021) 106531.
[41] C. Prieto, M. Cimmino, Transient multipole expansion for heat transfer in ground heat exchangers, Sci. Technol. Built Environ. 27 (2021) 253–270.
[42] D. Rohde, T. Andresen, N. Nord, Analysis of an integrated heating and cooling system for a building complex with focus on long–term thermal storage, Appl. Therm. Eng. 145 (2018) 791–803.
[43] G. Hellström, DST Duct ground storage model, Man. Comput. Code. (1989) 157
[44] E. Atam, L. Helsen, A convex approach to a class of non-convex building HVAC control problems: illustration by two case studies, Energy Build. 93 (2015) 269–281.
[45] T. Sivasakthivel, K. Murugesan, H.R. Thomas, Optimization of operating parameters of ground source heat pump system for space heating and cooling by Taguchi method and utility concept, Appl. Energy. 116 (2014) 76–85.
[46] F. Reda, Long term performance of different SAGSHP solutions for residential energy supply in Finland, Appl. Energy 144 (2015) 31–50.
[47] G. Nouri, Y. Noorollahi, H. Yousefi, Designing and optimization of solar assisted ground source heat pump system to supply heating, cooling and hot water demands, Geothermics 82 (2019) 212–231.
[48] D. Rohde, B.R. Knudsen, T. Andresen, N. Nord, Dynamic optimization of control setpoints for an integrated heating and cooling system with thermal energy storages, Energy 193 (2020) 116771.
[49] F. Ruiz-Calvo, C. Montagud, A. Cazorla-Marín, J.M. Corberán, Development and experimental validation of a TRNSYS dynamic tool for design and energy optimization of ground source heat pump systems, Energies 10 (2017) 1510.
[50] H. Li, J. Hou, T. Hong, Y. Ding, N. Nord, Energy, economic, and environmental analysis of integration of thermal energy storage into district heating systems using waste heat from data centres, Energy 219 (2021) 119582.
[51] I. Cupeiro Figueroa, M. Cimmino, L. Helsen, A methodology for long-term model predictive control of hybrid geothermal systems: the shadow-cost formulation, Energies 13 (2020).
[52] S.R. Mohandes, X. Zhang, A. Mahdiyar, A comprehensive review on the application of artificial neural networks in building energy analysis, Neurocomputing 340 (2019) 55–75.
[53] M. Mohanraj, S. Jayaraj, C. Muraleedharan, Applications of artificial neural networks for refrigeration, air-conditioning and heat pump systems—a review, Renew. Sustain. Energy Rev. 16 (2012) 1340–1358.
[54] H. Esen, M. Inalli, Modelling of a vertical ground coupled heat pump system by using artificial neural networks, Expert Syst. Appl. 36 (2009) 10229–10238.
[55] W. Sun, P. Hu, F. Lei, N. Zhu, Z. Jiang, Case study of performance evaluation of ground source heat pump system based on ANN and ANFIS models, Appl. Therm. Eng. 87 (2015) 586–594.
[56] J.-L. Fannou, C. Rousseau, L. Lamarche, S. Kajl, Modeling of a direct expansion geothermal heat pump using artificial neural networks, Energy Build. 81 (2014) 381–390.
[57] B. Dusseault, P. Pasquier, Efficient g-function approximation with artificial neural networks for a varying number of boreholes on a regular or irregular layout, Sci. Technol. Built Environ. 25 (2019) 1023–1035.
[58] W. Gang, J. Wang, Predictive ANN models of ground heat exchanger for the control of hybrid ground source heat pump systems, Appl. Energy 112 (2013) 1146–1153.
[59] D. Lee, R. Ooka, S. Ikeda, W. Choi, Artificial neural network prediction models of stratified thermal energy storage system and borehole heat exchanger for model predictive control, Sci. Technol. Built Environ. 25 (2019) 534–548.
[60] A.R. Puttige, S. Andersson, R. Östin, T. Olofsson, A novel analytical-ANN hybrid model for borehole heat exchanger, Energies 13 (2020) 6213.
[61] A.R. Puttige, S. Andersson, R. Östin, T. Olofsson, Application of regression and ANN models for heat pumps with field measurements, Energies 14 (2021), https://doi.org/10.3390/en14061750.
[62] A.R. Puttige, Utilization of a GSHP System in a DHC Network : modeling and optimization, Umeå University, 2021. http://umu.diva-portal.org/smash/get/diva2:1596121/FULLTEXT01.pdf.

[63] A.R. Puttige, S. Andersson, R. Östin, T. Olofsson, Improvement of borehole heat exchanger model performance by calibration using measured data, J. Build. Perform. Simul. 13 (2020) 430–442.
[64] T.S. Khan, M.S. Khan, M.-C. Chyu, Z.H. Ayub, Experimental investigation of single phase convective heat transfer coefficient in a corrugated plate heat exchanger for multiple plate configurations, Appl. Therm. Eng. 30 (2010) 1058–1065.
[65] NordPool, (n.d.). https://www.nordpoolgroup.com/historical-market-data/ (accessed April 27, 2021).